Article

Plagioclase zonation styles in hornblende gabbro inclusions from Little Glass Mountain, Medicine Lake volcano, California: implications for fractionation mechanisms and the formation of composition gaps

BROPHY, J.G., *et al*.

Abstract

The rhyolite of Little Glass Mountain (73–74% SiO_2) is a single eruptive unit that contains inclusions of quenched andesite liquid (54–61% SiO_2) and partially crystalline cumulate hornblende gabbro (53–55% SiO_2). Based on previous studies, the quenched andesite inclusions and host rhyolite lava are related to one another through fractional crystallization and represent an example of a fractionation-generated composition gap. The hornblende gabbros represent the cumulate residue associated with the rhyolite-producing and composition gap-forming fractionation event. This study combines textural (Nomarski Differential Interference Contrast, NDIC, imaging), major element (An content) and trace element (Mg, Fe, Sr, K, Ti, Ba) data on the style of zonation of plagioclase crystals from representative andesite and gabbro inclusions, to assess the physical environment in which the fractionation event and composition gap formation took place. The andesite inclusions (54–61% SiO_2) are sparsely phyric with phenocrysts of plagioclase, augite and Fe-oxide±olivine, +/–orthopyroxene, +/–hornblende set within a glassy [...]

Reference

BROPHY, J.G., *et al*. Plagioclase zonation styles in hornblende gabbro inclusions from Little Glass Mountain, Medicine Lake volcano, California: implications for fractionation mechanisms and the formation of composition gaps. *Contributions to Mineralogy and Petrology*, 1996, vol. 126, no. 1-2, p. 121-136

DOI : 10.1007/s004100050239

Contrib Mineral Petrol (1996) 126: 121–136

James G. Brophy · Michael J. Dorais
Julie Donnelly-Nolan · Bradley S. Singer

Plagioclase zonation styles in hornblende gabbro inclusions from Little Glass Mountain, Medicine Lake volcano, California: implications for fractionation mechanisms and the formation of composition gaps

Received: 28 December 1995 / Accepted: 24 July 1996

Abstract The rhyolite of Little Glass Mountain (73–74% SiO_2) is a single eruptive unit that contains inclusions of quenched andesite liquid (54–61% SiO_2) and partially crystalline cumulate hornblende gabbro (53–55% SiO_2). Based on previous studies, the quenched andesite inclusions and host rhyolite lava are related to one another through fractional crystallization and represent an example of a fractionation-generated composition gap. The hornblende gabbros represent the cumulate residue associated with the rhyolite-producing and composition gap-forming fractionation event. This study combines textural (Nomarski Differential Interference Contrast, NDIC, imaging), major element (An content) and trace element (Mg, Fe, Sr, K, Ti, Ba) data on the style of zonation of plagioclase crystals from representative andesite and gabbro inclusions, to assess the physical environment in which the fractionation event and composition gap formation took place. The andesite inclusions (54–61% SiO_2) are sparsely phyric with phenocrysts of plagioclase, augite and Fe-oxide + olivine, +/–orthopyroxene, +/–hornblende set within a glassy to crystalline matrix. The gabbro cumulates (53–55% SiO_2) consist of an interconnected framework of plagioclase, augite, olivine, orthopyroxene, hornblende and Fe-oxide along with highly vesicular interstitial glass (70–74% SiO_2). The gabbros record a two-stage crystallization history of plagioclase+olivine+augite (Stage I) followed by plagioclase+orthopyroxene+ hornblende+Fe-oxide (Stage II). Texturally, the plagioclase crystals in the andesite inclusions are characterized by complex, fine-scale oscillatory zonation and abundant dissolution surfaces. Compositionally (An content) the crystals are essentially unzoned from core-to-rim. These features indicate growth within a dynamic (convecting?), reservoir of andesite magma. In contrast, the plagioclase crystals in the gabbros are texturally smooth and featureless with strong normal zonation from An_{74} at the core to around An_{30}. K, and Ba abundances increase and Mg abundances decrease steadily towards the rim. Ti, Fe, and Sr abundances increase and then decrease towards the rim. The trace element variations are fully consistent with the two-stage crystallization sequence inferred from the gabbro mineralogy. These results indicate progressive closed-system in situ crystallization in a quiescent magmatic boundary layer environment located along the margins of the andesite magma body. The fractional crystallization that generated the host rhyolite lava is one of inward solidification of a crystallizing boundary layer followed by melt extraction and accumulation of highly evolved interstitial liquid. This mechanism explains the formation of the composition gap between parental andesite and rhyolite magma compositions.

J. G. Brophy (✉) · M. J. Dorais
Department of Geological Sciences, Indiana University, Bloomington, Indiana

J. Donnelly-Nolan
United States Geological Survey, Menlo Park, California

B. S. Singer
Department of Mineralogy, University of Geneva, Switzerland

Editorial responsibility: T. Grove

Introduction

Fractionation-generated composition gaps are a notable feature of volcanic systems in many different tectonic environments including subduction zones (e.g. Gerlach and Grove 1982; Hildreth 1983; Crawford et al. 1987; Bacon and Druitt 1988; Brophy 1991), back-arc environments (Weaver et al. 1979), continental rifts (Baker et al. 1977; Weaver 1977; MacDonald 1987), continental flood basalt provinces (Thompson 1972), and oceanic islands (Daly 1925). Given that fractional crystallization generates a continuous rather than discontinuous range of liquid compositions, the presence of a composition gap among erupted lavas and/or pyroclastics is most likely due to some physical process that prohibits a certain range of magma compositions from erupting. Thus, understanding the formation of fractionation-generated composition gaps may be a key to understanding the

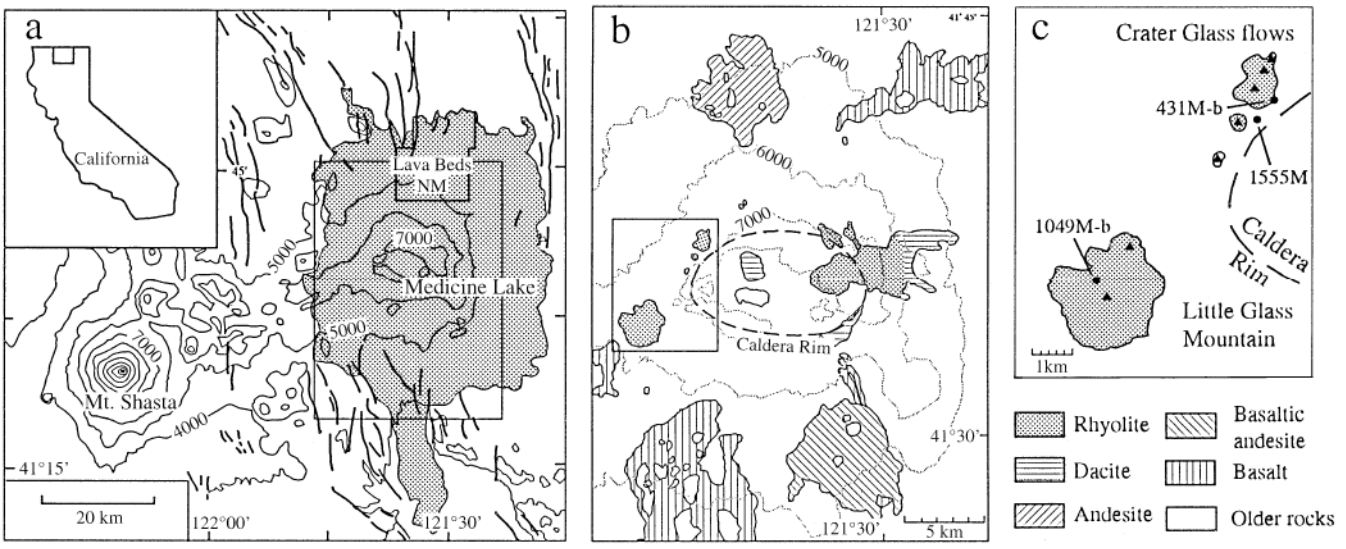

Fig. 1a–c Location map from Donnelly-Nolan (1988) showing **a** the location of Medicine Lake volcano (*shaded area*); **b** an enlarged view of the central portion of the volcano showing the locations of various late-Holocene basalt to rhyolite eruptive events; and **c** a further enlarged view of the Little Glass Mountain and Crater Glass lava flows along with the locations of hornblende gabbro cumulate inclusions 431M-b and 1555 M, and quenched andesite inclusion 1049M-b. The *heavy lines* in **a** show the locations of faults throughout the region. The *solid triangles* indicate the locations of specific vents or vent areas

physical aspects of fractionational crystallization in general. Medicine Lake volcano, located in the southern Cascade Range of northern California east of the main volcanic axis (Fig. 1) is a Pleistocene to Holocene shield volcano that has a well-defined fractionation-generated composition gap between high-SiO_2 andesite (61% SiO_2) and rhyolite (73% SiO_2). The late Holocene rhyolite of Little Glass Mountain consists of several flows and domes aligned along a NE-trend, including the Crater Glass flows (Fig. 1). The unit contains numerous inclusions of quenched andesite liquid (Mertzmann and Williams 1981). Grove and Donnelly-Nolan (1986) demonstrated that the host rhyolite lava was generated by fractional crystallization of a parental andesite magma that was similar to the quenched andesite liquid inclusions. The parental andesite inclusions and host rhyolite lava are one example of the Medicine Lake composition gap. Also present are hornblende gabbro inclusions that represent samples of the cumulates from the actual (or similar) fractional crystallization event that produced the host rhyolite (Grove and Donnelly-Nolan 1986). The occurrence of a parental magma and fractionation-generated derivative magma that define a fractionation-generated composition gap, along with the cumulates associated with the formation of the gap, provides an opportunity to assess the physical environment in which the fractional crystallization and gap formation took place.

Based on the assumption that crystal zonation styles preserve a record of the physical magmatic environment during crystal growth, this study presents a combined textural (Nomarski Differential Interference Contrast, NDIC, Imaging) and compositional (electron and ion microprobe) analysis of plagioclase zonation styles in both the parental magma (quenched andesite inclusions) and fractionation-generated cumulate (hornblende gabbro inclusions). Our results illustrate that the fractional crystallization event that generated the rhyolite magma occurred primarily through closed system in situ factionation within a thermal magmatic boundary layer (i.e. solidification front) located somewhere along the margins of an andesitic magma body. Eruption of non-fractionated parental andesite, coupled with extraction and eruption of highly evolved rhyolitic melt from within the boundary layer, is responsible for the formation of the Little Glass Mountain composition gap.

Medicine Lake Volcano and the rhyolite of Little Glass Mountain: geologic setting and previous work

Medicine Lake volcano lies in a predominantly E-W extensional setting that reflects the impingement of basin and range style extensional faulting on the main Cascade volcanic arc to the west. Late Holocene mafic and silicic lavas have erupted through vents that define roughly linear vent systems typically oriented NNW to NNE and parallel to the trend of major faults in the region (Fig. 1). Different aspects of the geology of Medicine Lake volcano have been studied by numerous authors (Powers 1932; Anderson 1933 1941; Eichelberger 1975 1981; Condie and Hayslip 1975; Mertzmann 1977a, b; Heiken 1978; Mertzmann and Williams 1981; Ciancanelli 1983). More recent papers include detailed petrologic work by Grove and co-workers (Grove et al. 1982 1988; Gerlach and Grove 1982; Grove and Donnelly-Nolan 1986; Donnelly-Nolan et al. 1991; Wagner et al. 1995)) and a summary of the geology and geochronology of the volcano by Donnelly-Nolan (1988) and Donnelly-Nolan et al. (1990). Grove and co-workers have demonstrated that the spectrum of basalt to rhyolite lava compositions can be derived from parental tholeiitic basalt by a combination of processes including fractional crystallization, assimilation of granitic crustal material, and magma mixing.

The rhyolite of Little Glass Mountain is one of several late Holocene units at Medicine Lake volcano that contain inclusions (e.g. Mertzmann and Williams 1981; Eichelberger 1981; Grove

and Donnelly-Nolan 1986; Grove et al. 1988). At Little Glass Mountain, quenched magmatic inclusions of basaltic and andesitic compositions are the most common, but gabbros of presumed cumulate origin are also present. Fragments of partially fused granite are also present. Grove and Donnelly-Nolan (1986) studied these inclusions in detail and convincingly demonstrated that: (1) the hornblende gabbro inclusions represent the cumulate residue of a fractionation event that produced a rhyolite similar or identical to the host rhyolite of Little Glass Mountain; (2) the parental magma from which the cumulate hornblende gabbros were derived was a low-SiO_2 andesite (¥56 wt% SiO_2) that is similar to many of the quenched andesite inclusions; and (3) the fractionation process was accompanied by selective assimilation (up to and perhaps more than 30% by weight; Donnelly-Nolan, unpublished data) of granitic wall rock that is now represented by the partially fused granite xenoliths. These conclusions, which are ultimately supported in full by our study, form the initial working premise for much of the work discussed below. For more specific information, the reader is referred to Grove and Donnelly-Nolan (1986).

Analytical techniques

Polished thin sections were etched in fluoro-boric acid, HBF_4, for 25–30 s and then studied with reflected light NDIC microscopy. Major element analyses of plagioclase phenocrysts were conducted on a four-spectrometer Cameca SX-50 electron microprobe located at the Department of Geological Sciences, Indiana University. Standard operating conditions included a 15 kV accelerating voltage, 15 nA sample current, and 10 s counting times for all elements. A spot size of 2 mm was used for plagioclase, while a defocused 20 mm wide beam was used for glass. To minimize Na-loss due to volatilization or diffusion, Na was always counted

Table 1 Whole rock geochemical data (*n.d.* not determined)[a]

	431M-b Gabbro	1012M-d Gabbro	1025M-c Gabbro	1025M-d Gabbro	1043M Gabbro	1555M Gabbro	366M-b Andesite	1025M-h Andesite	366M-b Andesite	1042M-a Andesite	1012M-b Andesite	1049M-b Andesite
SiO_2	52.9	55.00	53.70	53.40	53.30	53.2	54.8	54.6	54.8	58.7	58.0	56.4
TiO_2	0.81	0.86	0.86	0.80	0.81	0.86	0.79	0.83	0.79	1.10	0.75	0.77
Al_2O_3	19.10	18.00	17.90	19.40	18.40	18.60	18.10	18.20	18.10	17.00	17.30	17.60
Fe_2O_3	0.69	0.77	0.81	0.75	0.81	0.74	0.69	0.71	0.69	0.72	0.62	0.65
FeO[b]	6.19	6.20	6.56	6.05	6.52	6.70	6.20	6.36	6.20	6.48	5.54	5.81
MnO	0.12	0.12	0.13	0.12	0.13	0.13	0.12	0.13	0.12	0.12	0.11	0.11
MgO	5.82	5.45	5.71	5.60	6.14	6.08	5.65	5.52	5.65	3.06	4.73	5.17
CaO	9.64	8.68	9.69	9.69	9.49	9.21	8.61	9.18	8.61	6.61	7.42	7.92
Na_2O	3.09	3.24	3.21	3.05	3.03	3.24	3.08	2.98	3.08	3.75	3.40	3.31
K_2O	0.76	1.03	0.73	0.80	0.79	0.75	1.19	0.93	1.19	1.73	1.58	1.33
P_2O_5	0.18	0.17	0.17	0.17	0.16	0.18	0.14	0.17	0.14	0.24	0.14	0.14
LOI	0.00	0.31	0.31	0.16	n.d.	0.16	0.03	0.21	0.03	0.24	0.41	0.63
Total	99.3	100.21	100.20	100.50	100.30	99.69	99.37	99.61	99.37	99.51	99.59	99.2
Mg#[c]	63	62	61	63	63	62	62	61	62	46	61	62
Rb	21	28	16	19	16	22	32	25	32	51	48	121
Sr	490	419	448	477	460	504	428	442	428	390	376	383
Ba	261	298	260	255	252	253	293	267	293	440	369	348

	1235M-Andesite	1554M Andesite	1121M Rhyolite	1329M Rhyolite	532M-a Glass	647-M Glass	661M-c Glass	1-25M-d Glass	431M-b Glass	1012M-c Glass	1555M Glass
SiO_2	59.0	55.2	73.8	73.6	76.21	75.40	74.40	71.07	70.46	75.93	70.34
TiO_2	1.34	0.84	0.27	0.26	0.29	0.17	0.36	0.45	0.42	0.21	0.41
Al_2O_3	16.00	17.50	13.7	13.7	12.96	13.65	13.80	15.47	15.68	13.26	15.43
Fe_2O_3	0.74	0.71	0.17	0.17	n.d.	n.d.	n.d.	n.d.	n.d.	n.d.	n.d.
FeO[b]	6.63	6.37	1.56	1.49	1.18	0.98	1.71	2.36	2.57	1.03	2.72
MnO	0.14	0.13	0.02	0.02	0.03	0.06	0.06	0.08	0.07	0.05	0.11
MgO	2.58	5.13	0.33	0.30	0.11	0.07	0.14	0.38	0.40	0.08	0.47
CaO	5.61	8.68	1.28	1.26	0.36	0.76	0.52	1.81	1.87	0.46	1.80
Na_2O	4.47	3.14	3.98	3.98	3.10	3.83	3.57	5.64	5.26	3.37	4.85
K_2O	1.79	1.10	4.35	4.36	5.35	4.51	5.09	2.01	2.46	5.00	2.85
P_2O_5	0.35	0.14	0.00	0.00	0.13	0.04	0.12	0.16	0.13	0.06	0.12
LOI	0.36	0.01	0.19	0.31	n.d.	n.d.	n.d.	n.d.	n.d.	n.d.	n.d.
Total	98.65	98.94	99.46	99.13	99.72	99.46	99.76	99.42	99.31	99.45	99.09
Mg#	41	59	28	27	15	11	13	22	22	12	24
Rb	51	34	160	132	n.d.	n.d.	n.d.	n.d.	n.d.	n.d.	n.d.
Sr	330	451	143	132	n.d.	n.d.	n.d.	n.d.	n.d.	n.d.	n.d.
Ba	530	321	890	820	n.d.	n.d.	n.d.	n.d.	n.d.	n.d.	n.d.

[a] Analysts (major elements): J.S. Wahlberg, J. Taggart, J. Baker, A.J. Bartel, K. Stewart, R.V. Mendes, D. Siems, USGS, Lakewood, CO. Analysts (trace elements): R. Johnson, H.J. Rose, B. McCall, G. Sellers, J. Lindsley, USGS Reston, VA, and P. Bruggman, USGS Menlo Park, CA.
[b] $FeO=0.9*(FeO+Fe_2O_3)$
[c] $Mg\#=Mg/(Mg+Fe^{2+})$

first. Automatic core to rim traverses across plagioclase were conducted by selecting the beginning and end points of the traverse and then setting the number of analyses such that a 4-mm interval between spots was maintained throughout. Raw counts were converted to oxide concentrations using the on-line PAP correction scheme of Pouchou and Pichoir (1985). Trace (K, Ti, Sr, Ba) and minor (Mg, Fe) element concentrations in plagioclase were determined by secondary ion mass spectrometry (SIMS) on a Cameca IMS 3f ion microprobe located at the Woods Hole Oceanographic Institute. The primary O beam was focused to a spot diameter of approximately 15 mm. For each analysis, intensities of ^{24}Mg, ^{28}Si, ^{39}K, ^{40}Ca, ^{47}Ti, ^{58}Fe, ^{88}Sr , and ^{138}Ba were measured five times. Each intensity measurement was converted to an intensity ratio by dividing by ^{28}Si. Average intensity ratios were then converted to element abundance using empirical calibration curves determined for each element (Shimizu and Hart 1982). Typical relative standard deviations (RSD, 2s) for element abundances are Mg (1.5%), K (2.75%), Ti (3.62%), Fe (2.0%), Sr (4.25%), and Ba (3.5%). Analyses with a RSD>10% were excluded. Automatic core-to-rim analyses were conducted by selecting the beginning and end points and then setting the number of analyses such that an analysis interval of either 4 or 5 mm was maintained throughout. Because this interval is less than the diameter of the primary O beam, adjacent analyses overlapped with one another. Due to the large width of the primary beam, analyses within 15 mm of the crystal rim showed interference from the surrounding matrix.

Host rhyolite, hornblende gabbro, and quenched andesite inclusions: geochemistry, petrography and mineralogy

Table 1 lists major element and selected trace element (Rb, Sr, Ba) compositions of numerous host rhyolite lava samples, hornblende gabbro inclusions and interstitial glass, quenched andesite inclusions, and granitic xenoliths. Additional data can be found in Grove and Donnelly-Nolan (1986). The host rhyolite lava consists of obsidian and pumice that ranges from 73 to 74% SiO_2 . The obsidians contain less than 1 vol.% phenocrysts of plagioclase, orthopyroxene, and Fe-oxides set within a matrix of glass and flow-aligned plagioclase microlites. Microphenocrysts of hornblende and apatite are rarely present. The phenocrysts are all rounded and embayed in appearance. Mineral analyses have been reported by several investigators (Smith and Carmichael 1968; Mertzman and Williams 1981; Gerlach and Grove 1982).

The hornblende gabbros range from 53 to 55 wt% SiO_2 and have Mg#s that range from 59 to 63. All gabbros consist of an interconnected crystalline network of plagioclase, augite, hornblende, orthopyroxene, olivine, and Fe-oxide (magnetite and ilmenite) set within a matrix of highly vesicular light- to dark-brown glass. Modal analyses of several gabbros are given in Table 2. Photomicrographs of two typical gabbros can be found in Grove and Donnelly-Nolan (1986). Small crystals of apatite and zircon, as well as quench crystals of plagioclase are distributed throughout the glass portion of many samples. The interstitial glass is rhyolitic in composition (70 to 75% SiO_2, Table 1) and is similar to the composition of the host rhyolite lava . Grove and Donnelly-Nolan (1986) inferred a two-stage crystallization sequence starting with early cotectic crystallization of olivine +augite+plagioclase (Stage I) followed by reaction of olivine and augite with the liquid to produce orthopyroxene and hornblende respectively and continued crystallization of plagioclase + orthopyroxene + hornblende + Fe-oxide + apatite (Stage II).

Table 2 Modal analyses of selected hornblende gabbros[a]

	431M-b	1555M	1012M-c[b]	661M-c[b]	532M-a[b]
Olivine	2	3	2	1	1
Plagioclase	34	37	50	42	49
Augite	8	9	7	8	11
Opx	2	4	4	3	3
Amphibole	8	8	19	20	11
Fe-Oxide	2	1	1	1	1
Glass	44	38	17	25	24

[a] Volume percentages based on 1000 pts/slide
[b] Chemical Data in Grove and Donnelly-Nolan (1986)

The andesites range from 54 to 61 wt% SiO_2 and are aphyric to sparsely porphyritic in texture. Photomicrographs of typical andesite inclusions can be found in Grove and Donnelly-Nolan (1986). These authors classified the inclusions as: low SiO_2 (54–57%, olivine+plagioclase+augite), intermediate SiO_2 (58–60%, orthopyroxene, plagioclase, Fe-oxide, +/–hornblende) and high SiO_2 (>60%, orthopyroxene, hornblende, plagioclase, Fe-oxide). Rare xenocrysts of iron-rich orthopyroxene and both calcic and sodic plagioclase are present in many samples.

Hornblende gabbros 1555 M and 431M-b, and andesite inclusion 1049M-b: textural, major element and trace element zonation styles

Two representative hornblende gabbro inclusions and one quenched andesite inclusion were selected for detailed study. The two hornblende gabbros (1555M and 431M-b) are from the Crater Glass flows (Fig. 1) and are representative of the more mafic end of the gabbro compositional spectrum (Mg# 62–63). Gabbro 1555M was sampled from an ejected pumice block adjacent to the southern Crater Glass flow. Gabbro (431M-b) was studied by Grove and Donnelly-Nolan (1986). Compositionally, texturally, and mineralogically the two gabbros are identical. The one quenched andesite inclusion (1049M-b) is from Little Glass Mountain and belongs to the low-SiO_2 andesite group of Grove and Donnelly-Nolan (1986) with around 56.5 wt% SiO_2.This SiO_2 value is close to that of the parental andesite magma predicted by Grove and Donnelly-Nolan (1986). It contains phenocrysts of plagioclase, olivine, clinopyroxene, and rare Fe-oxide.

Fifty plagioclase cores were analyzed in the gabbro inclusions, and around 40 cores were analyzed in the andesite inclusion. The two gabbro inclusions display a bi-modal distribution of plagioclase core compositions (Fig. 2). Obvious xenocrystic cores define a high-An

population of An_{80} to An_{84}. Most crystals lack xenocrystic cores and define an intermediate-An population of An_{76} to An_{50}. Plagioclase crystals that contain An-rich, xenocrystic cores will be referred to as *Type A* plagioclase whereas those that belong to the intermediate-An population will be referred to as *Type B* plagioclase. The andesite inclusion posesses a single population of intermediate-An plagioclase phenocrysts that fall between An_{67} and An_{76}. It is noteworthy, that the composition of the most An-rich andesite phenocryst corresponds precisely with that of the most An-rich Type B plagioclase crystal in both gabbro cumulates. The andesite inclusion also contains a small number of more sodic crystals in the An_{30} to An_{50} range.

Plagioclase textures in all three inclusions were examined with NDIC microscopy. Numerous crystals were thereby selected for detailed major element (mol% An) core-to-rim electron microprobe analysis. The results show that, within a given sample (gabbro or andesite), and within a given crystal group (Type A cumulate, Type B cumulate, andesite phenocryst) the zoning styles are nearly identical. Among the different groups, however, several important differences exist. Figure 3 shows

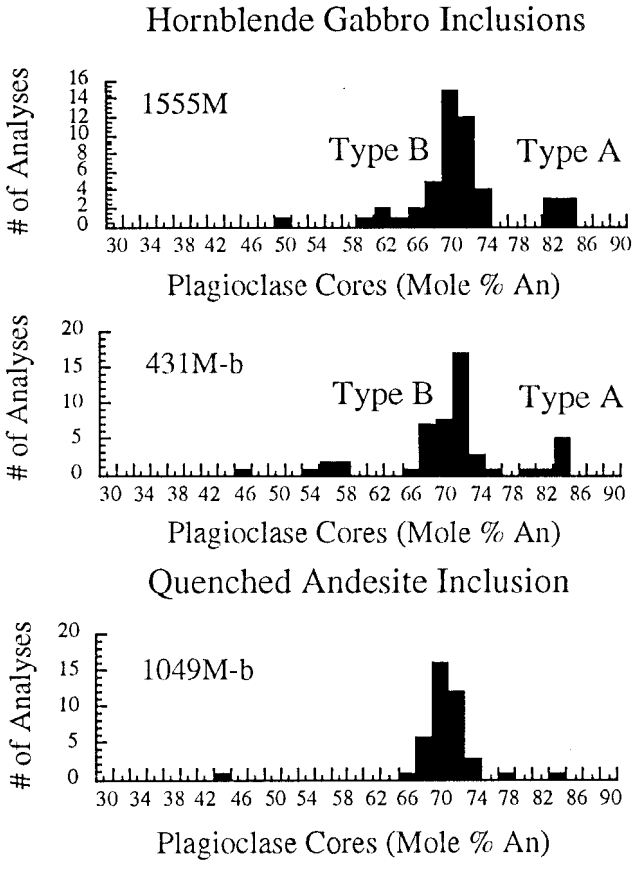

Fig. 2 Histograms of plagioclase core compositions from hornblende gabbro cumulate inclusions 1555M and 431M-b (n=50/sample), and the low-SiO_2 andesite inclusion 1049M-b (n=40). In the hornblende gabbro cumulate inclusions, the Type A plagioclase crystals are defined as those that contain calcic xenocrystic cores whereas Type B crystals lack xenocrystic cores

NDIC images and major element (mol% An) core-to-rim traverses for representative Type A and Type B crystals from each of the two hornblende gabbro cumulates, and two representative phenocrysts from the andesite inclusion. We refer to these crystals as 1555M-A and 431M-b-A (Fig. 3a,b) indicating the Type A crystals from gabbro cumulates 1555M and 431M-b respectively, 1555M-B and 431M-b-B (Fig. 3c,d), indicating the Type B crystals, and 1049M-B-1 and 1049M-b-2 (Fig. 3e,f), indicating the two plagioclase phenocrysts from quenched andesite inclusion 1049M-b.

The two Type A crystals are very similar (Fig. 3a,b). In each case, an anhedral, calcic core (An_{75-89}) displays complex wavy and/or patchy zonation that is abruptly truncated by a surrounding mantle that is texturally smooth and featureless save for a few widely spaced NDIC zone boundaries. The mantles lack any evidence of crystal dissolution, resorption, and/or overgrowth. Both mantles display smooth normal zonation from An_{74} at the core-mantle boundary to around An_{45} (1555M-A) or An_{50} (431M-b-A) near the crystal rim. The various zone boundaries seen in the NDIC images are correlated with either very small (<2 mol% An) or non-detectable shifts in An content. The outermost portion of both mantles are truncated by a noticeable dissolution surface which forms the inner boundary of a very narrow quench rim of around An_{30}. The textural and compositional features of the two type B crystals are also nearly identical to one another (Fig. 3c,d). Both crystals are texturally smooth and featureless with relatively few zone boundaries and a complete lack of dissolution surfaces. Both crystals are normally zoned from core compositions of around An_{74} to rim compositions of around An_{45}, followed by a narrow quench rim of around An_{30}. In all respects, the Type B crystals are identical to the mantle of the Type A crystals in the same gabbro inclusion. The two andesite plagioclase phenocrysts (Fig. 3e,f) are markedly different from the Type A mantles and Type B crystals of the two gabbro cumulates. Both phenocrysts display complex, fine-scale oscillatory zoning throughout the entire crystal as indicated by numerous, closely spaced zone boundaries. Both crystals contain one or more dissolution surfaces accompanied by discontinuous changes in An content of <2 mol% to as great as 10 mol% An. Both crystals have a core composition of An_{70} and are largely unzoned throughout much of the crystal. Towards the rim, both crystals have a very slight reverse zonation followed by an abrupt quench zone at the rim.

In the two gabbro cumulates, the compositional range of the Type A xenocrystic cores (An_{80-87}) is much more An-rich than any of the phenocrysts observed in the low-SiO_2 andesite inclusions and thus indicates crystallization from a more mafic magma, presumably of basalt composition. The ultimate origin and significance of these calcic plagioclase xenocryst cores is not considered here. Since the compositional range and style of zonation in the Type B crystals is identical to that of the mantles of the Type A crystals, the Type A mantles and

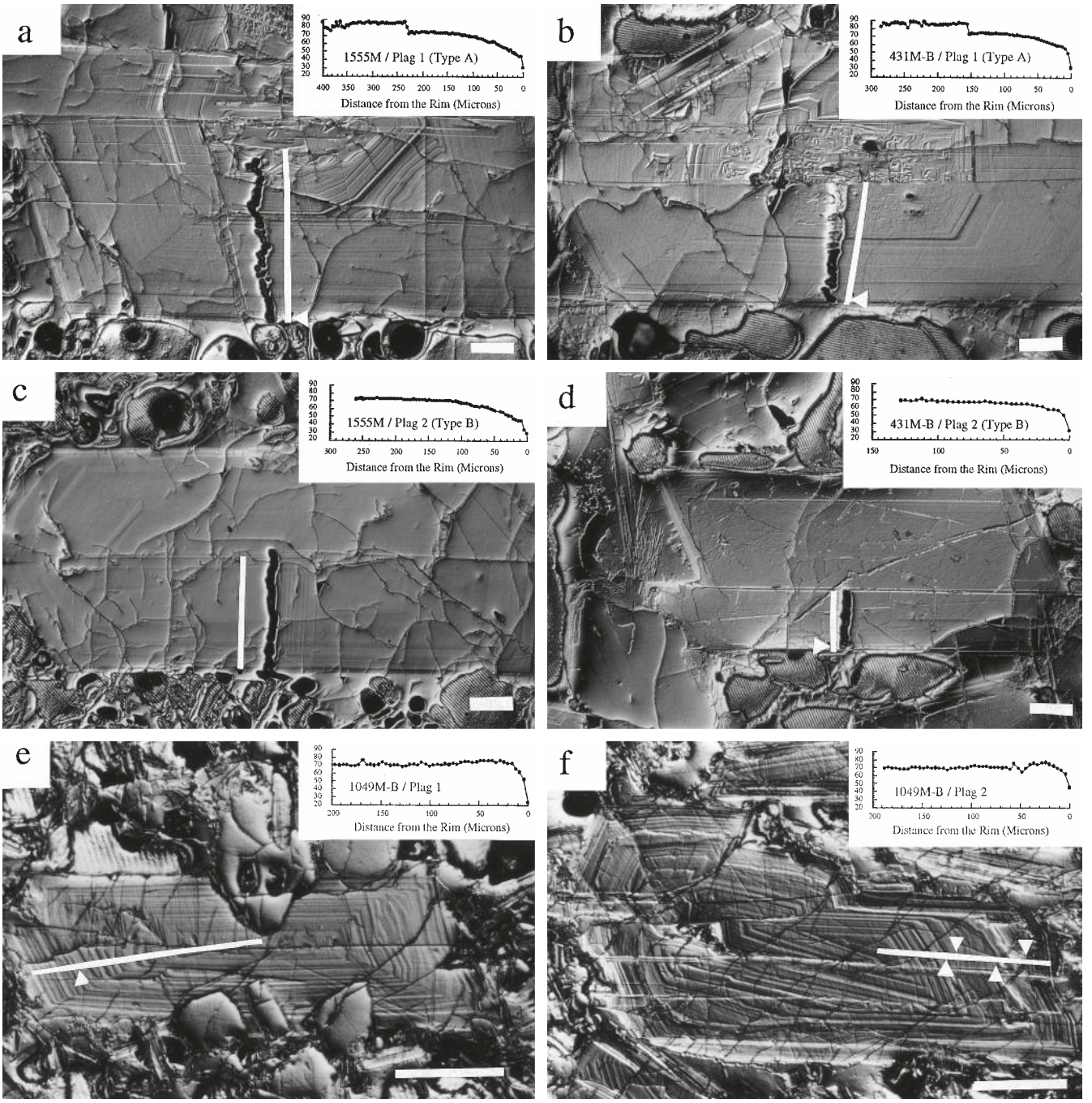

Fig. 3 NDIC images and accompanying core-to-rim electron microprobe (mol% An) zonation profiles of representative Type A and Type B plagioclase crystals from hornblende gabbro cumulates 1555M and 431M-b, and representative phenocrysts from the low-SiO_2 andesite inclusion 1049M-b. Specific crystals are: **a** 1555M-A; **b** 431M-b-A; **c** 1555M-B; **d** 431M-b-B; **e** 1049M-b-1; and **f** 1049M-b-2. In each image, the location of the microprobe traverse is indicated by a *solid white line*. In the four gabbro cumulate crystals, the location of the core-to-rim ion microprobe traverse is clearly visible near the white line. The horizontal white scale bar in the lower right corner is 100 m in length. The *white arrows* indicate the locations of minor and/or major dissolution surfaces

Type B crystals within a given gabbro inclusion have likely recorded the same period of crystallization from a liquid of the same composition. The most An-rich plagioclase that was formed during this period of crystallization (An_{74}) is similar to the most An-rich phenocrysts in andesite inclusion 1049M-b. This suggests, as previously concluded by Grove and Donnelly-Nolan (1986), that the parental magma that gave rise to the two gabbro cumulates was a low-SiO_2 andesite similar to some of the quenched inclusions.

The textural and compositional diversity of the andesite phenocrysts implies a dynamically complex growth history, such as one might expect in the interior of a

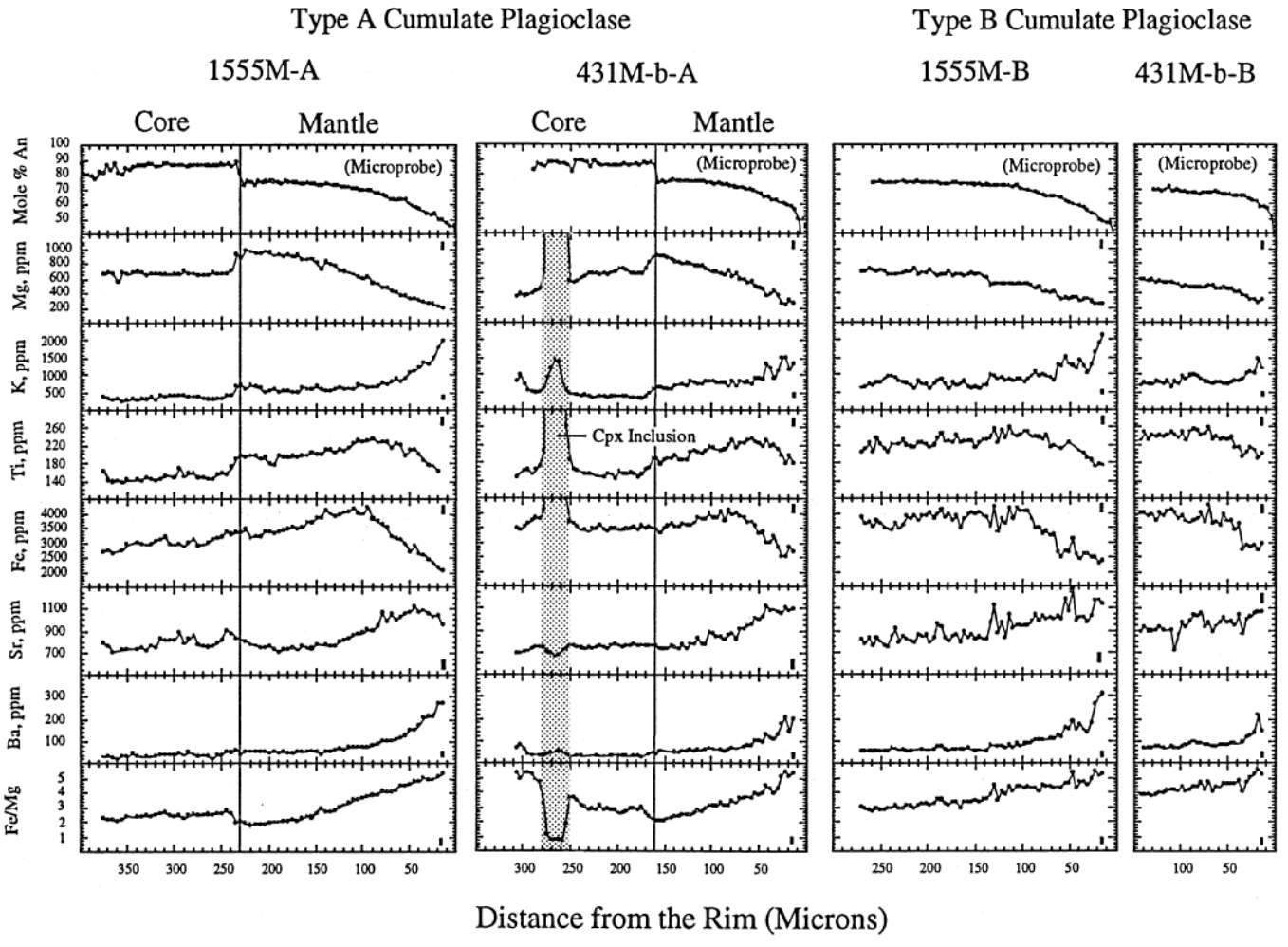

Fig. 4 Core-to-rim variations in major element (mol% An, electron microprobe) and selected trace element (Mg, K, Ti, Fe, Sr, Ba, ion microprobe) abundances in hornblende gabbro cumulate Type A crystals (1555M -A and 431M-b-A) and Type B crystals (1555M-B and 431M-b-B). The *vertical solid bars* on the far right side of each traverse indicate the maximum analytical uncertainty associated with individual trace element analyses. The analytical uncertainty in mol% An is smaller than the symbols. The *stippled area* in 431M-b-A indicates a small inclusion of clinopyroxene that was inadvertently included in the ion-probe traverse. Note that the horizontal and vertical scales are the same for all parts of the figure

convecting magma body (e.g. Pearce 1994; Singer et al. 1995) whereas the uniformity of the cumulate plagioclase crystals implies a more simple growth history. This, in turn, implies that the plagioclase crystals now found in the cumulate hornblende gabbros did not originate as free-floating phenocrysts in a parental low-SiO_2 andesite magma but, rather, were formed in an entirely different magmatic environment. As discussed below, we interpret this environment to be a stagnant thermal magmatic boundary layer (i.e. solidification front) located somewhere along the margins of the parental andesite magma body.

The four Type A and B crystals from the two gabbro inclusions were analyzed for selected trace elements (Mg, K, Ti, Fe, Sr, Ba) along core-to-rim profiles (Fig. 4). The ion microprobe traverses are clearly visible in the NDIC images of Figure 3. Due to the width of the primary O beam (¥15 ㎜), analyses within the outermost 15 ㎜ of all four crystals overlap the surrounding glass matrix and are therefore excluded from consideration. The two Type A crystals have similar variations in Mg, K, Ti, Fe, Sr, and Ba abundances. The calcic cores have somewhat variable element abundances whereas the mantles show smooth, systematic rim-ward variations in all element abundances. Going toward the rim, K and Ba abundances increase, Mg abundances decrease, and Ti, Fe, and Sr abundances initially increase and then decrease. As with An content, the Type B crystals have trace element variations that are very similar to the Type A mantles, futher supporting simultaneous growth from a liquid of the same composition. One difference between the Type A and Type B profiles is a second-order "sawtooth" variation superimposed on the latter. The potential significance of this feature is not considered here.

Discussion

An assessment of equilibrium vs non-equilibrium partitioning behavior

Equilibrium plagioclase-melt partition coefficients and measured plagioclase zoning profiles have been used to reconstruct the evolution of melts that produced the cumulate minerals in the gabbro xenoliths. Compelling evidence that favors near equilibrium trace element partitioning behavior is the similarity in zoning across the mantle of crystal 1555M-A and the entirety of 1555M-B.

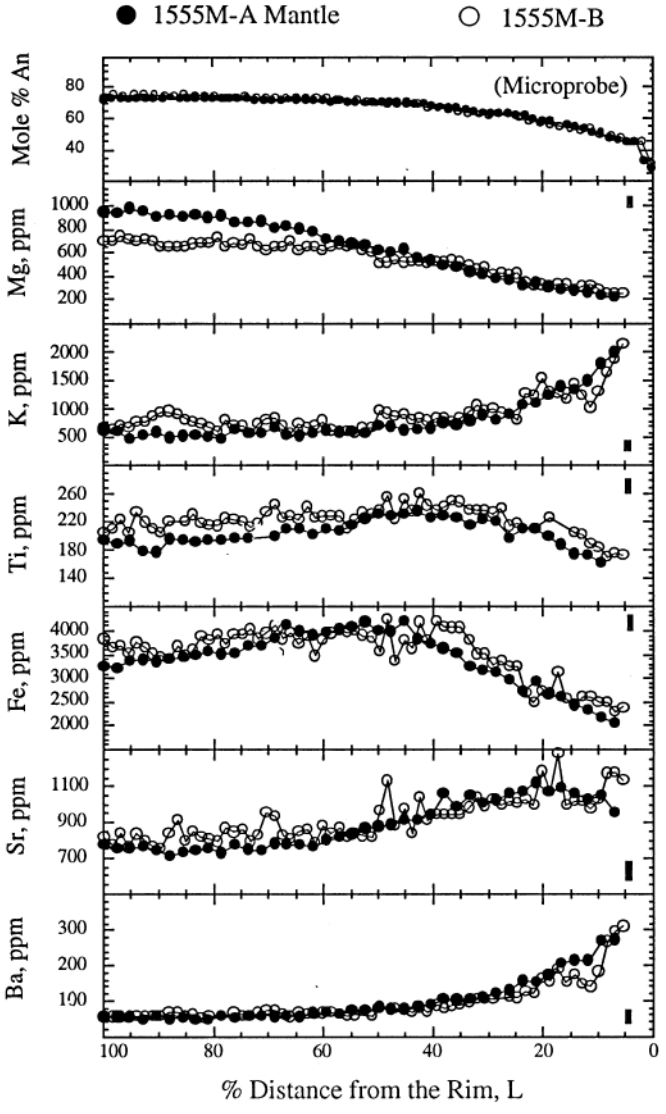

Fig. 5 A comparison of major element and trace element abundances in the mantle of 1555M-A and the entirety of 1555M-B versus the percentage distance from the rim, L, where L=(dist from the rim/total distance)*100. A given value of L is thought to represent the same period of crystal growth. The close similarity in absolute abundances and overall zonation profiles in the two different crystals is evidence that the major and trace element partitioning behavior during crystal growth approached that of equilibrium conditions

The two crystals appear to have grown over the same period from the same progressively fractionating liquid. If the growth rate of the two crystals was about the same, then any two points at the same relative distance across the two crystals should have formed from the same period of crystal growth and should have similar chemical characteristics. Figure 5 shows that this is indeed the case. The overall trend and absolute elemental abundances are nearly identical in each of the two crystals. The one exception is Mg, which displays significantly lower abundances in crystal 1555M-B for the initial half of the zoning profile, but is nearly identical in the outer half of the crystal. There is nearly exact correspondence of the inflection point in the Fe and Ti profiles about 55% of the way to the rim and a possible correspondence of an inflection point in the Sr profile about 90% of the way to the rim. These results indicate that, at a given period of plagioclase crystallization, the operative plagioclase-liquid partition coefficient for a given major or trace element was the same for both crystals, despite the fact that they are separated from one another by a distance of 1.3 cm which is at least one order of magnitude greater than the diameter of the crystals themselves. This implies that major and trace element partitioning occurred under near equilibrium conditions.

Reconstruction of the liquid-line-of-descent during parental andesite fractionation: Predicted SiO2, FeO, MgO, Sr and Ba abundances in the liquid

In this section the variations in liquid SiO_2, FeO, MgO, Sr and Ba during fractional crystallization are reconstructed and then compared with the corresponding observed abundances in the rhyolite of Little Glass Mountain. Given that the mantles of the Type A crystals have the smoothest zoning profiles and appear to have recorded the least amount of disequilibrium partitioning, all reconstructions of liquid composition are based on data from crystals 1555M-A and 431M-b-A. Liquid oxide (SiO_2, FeO, MgO) concentrations in wt% and trace element (Sr, Ba) abundances in ppm were predicted from the observed concentrations in plagioclase of An (mol%), Fe, Mg, Sr and Ba (in ppm) respectively as follows:

$$(SiO_2)_{liq} = -7.622\times10^{-5}(X_{An})^3_{plag} + 7.631\times10^{-3}(X_{An})^2_{plag} - 5.019\times10^{-1}(X_{An})_{plag} + 84.64 \quad (1)$$

$$(Sr)_{liq} = (Sr)_{plag} \cdot \exp\left(26{,}800/RT - 26{,}700\,(X_{An})_{plag}/RT\right) \quad (2)$$

$$(Ba)_{liq} = (Ba)_{plag} \cdot \exp\left(10{,}200/RT - 38{,}200\,(X_{An})_{plag}/RT\right) \quad (3)$$

$$(FeO)_{liq} = 0.0021 \cdot (Fe)_{plag} \quad (4)$$

$$(MgO)_{liq} = 0.0060 \cdot (Mg)_{plag} \quad (5)$$

The SiO_2-X_{An} relationship is based on an observed correlation between plagioclase composition and bulk rock SiO_2 content in late Holocene mafic to silicic lavas from Medicine Lake volcano (see Appendix). The Sr-X_{An} and Ba-X_{An} relationships are from Blundy and Wood

(1991) and assume a temperature of 950°C, which is based on the results of Fe-Ti oxide geothermometry (Grove and Donnelly-Nolan 1986). Liquid FeO and MgO abundances (wt%) were calculated from the observed Fe and Mg abundances in plagioclase (in ppm) through a constant partition factor chosen such that the innermost Fe and Mg concentrations (in ppm) in the mantle of 1555M predicted a liquid with FeO* and MgO abundances (in wt%) equivalent to that of the most primitive andesite inclusions (7.0% FeO* and 5.5% MgO). The corresponding Fe and Mg plagioclase/liquid partition coefficients are 0.063 and 0.028 respectively. The Fe partition coefficient is consistent with the experimental study of Longhi et al. (1976), who reported an average value of 0.058 (+/–0.008), as well as the more recent work of Sato (1989) and Phinney (1991) who showed that partition coefficient values between coexisting high-An plagioclase and basalt liquid vary from around 0.05 to 0.06 at f_O2 conditions along the QFM oxygen buffer to around 0.08 to 0.16 at f_O2 conditions of NNO + one log unit. The Mg partition coefficient is less than the experimentally determined values of 0.041, 0.042, and 0.043 reported by Longhi et al. (1976), Sato (1989), and Phinney (1991) respectively, but is within the range of values based on co-existing phenocryst-matrix pairs (0.026, 0.023, 0.03, and 0.018) reported by Sato (1989), Phinney and Morrison (1990), Meyer and Shibata (1990) and Brophy and Allan (1993) respectively.

Figure 6 shows the variations in liquid MgO, FeO*, Sr, and Ba versus SiO_2 as predicted from the mantles of crystals 1555M-A and 431M-b-A. Also shown are the observed compositions of the entire suite of quenched andesite inclusions and the four host rhyolite lava samples from Table 1 and Grove and Donnelly-Nolan (1986) for which MgO, FeO*, Sr and Ba data are available. The andesite inclusions define a field of decreasing MgO (5.65 to 2.24 wt%), FeO* (7.0 to 6.13 wt%) and Sr (572 to 311 ppm), and increasing Ba (267 to 624 ppm) over a SiO_2 range of 54.6 to 60.8 wt%. The four rhyolite samples range from 0.30 to 0.38 wt% MgO, 1.63 1.71 wt% FeO*, 118 to 143 ppm Sr and 803 to 890 ppm Ba over a very narrow SiO_2 range of 73.5–74.5 wt%. The initial (i.e. parental) liquid composition predicted from the two crystals is 57% SiO_2, 6.8 to 7.0% FeO, 4.2 to 5.5% MgO, 381 to 389 ppm Sr and 250 to 292 ppm Ba, all of which overlap the middle region of the andesite inclusion field. In all cases, the overall variations in the predicted liquid MgO, FeO*, Sr and Ba abundances trend *directly* towards the composition of the host rhyolite lava. This result indicates that the two hornblende gabbros have recorded a fractional crystallization event that produces rhyolitic liquids similar to that of the host rhyolite composition. Thus, on the basis of a completely different line of reasoning, our results confirm those of Grove and Donnelly-Nolan (1986) and demonstrate that the hornblende gabbros are indeed relevant to the fractionation process that generated the host rhyolite lava. Significantly, the maximum predicted SiO_2 values of 67% for 431M-b-A and 71% for 1555M-A, which agree favorably with the actual interstitial glass compositions of around

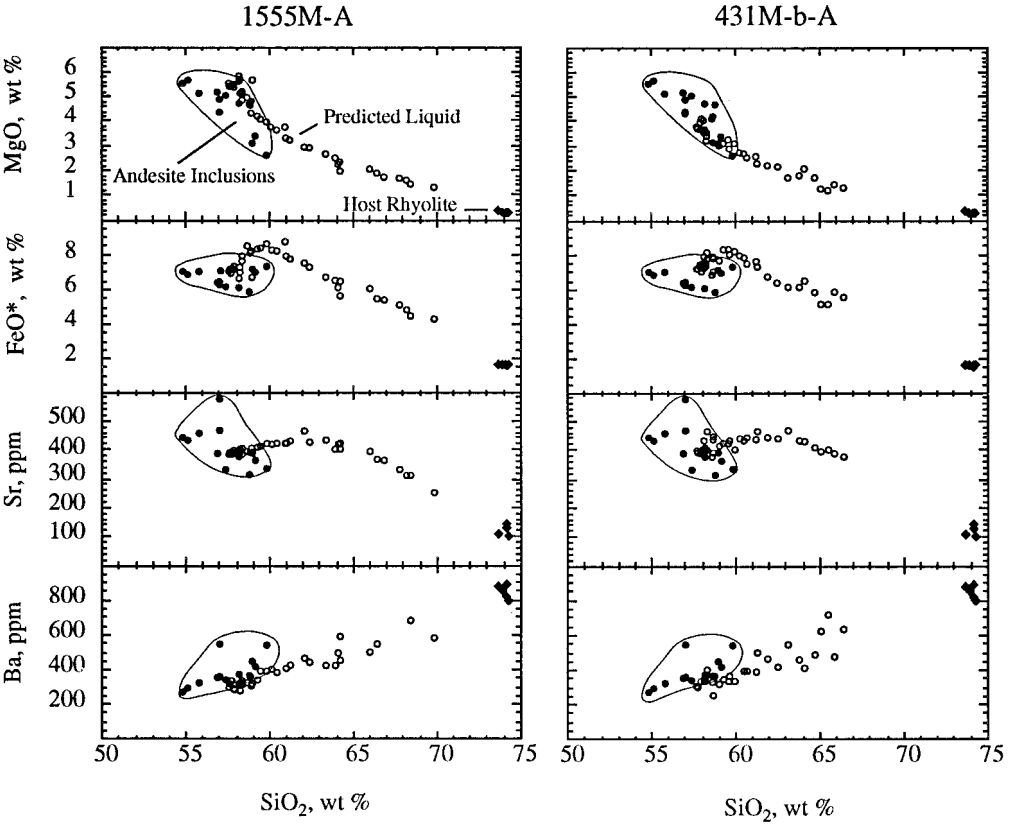

Fig. 6 Co-variations of liquid MgO and FeO* (in wt.%) and Sr and Ba (in ppm) with increasing SiO_2 as predicted from the mantles of 1555M-A and 431M-b-A. Also shown are the observed abundances of MgO, FeO*, Sr, and Ba in the quenched andesite inclusions and host rhyolite lava (from Table 1). The close agreement between the predicted least SiO_2-rich liquid and the field of quenched andesite inclusions supports the notion that the inclusions represent the parental andesite magma. With increasing SiO_2, the predicted liquid MgO, FeO*, Sr and Ba abundances trend *directly* towards the host rhyolite composition. This indicates that the fractional crystallization event recorded by the two hornblende gabbro cumulates is representative of the event that produced the host rhyolite lavas

70% SiO_2 for both inclusions, fall short of the 73–74% SiO_2 levels of the host rhyolite. If the two gabbros have recorded the same (or similar) fractionation event that generated the host rhyolite, then it is clear that neither sample has crystallized to the degree necessary to produce the host magma.

Hornblende gabbro plagioclase crystal zonation styles: evidence for in situ crystallization in a quiescent magmatic environment

The plagioclase phenocrysts in the low-SiO_2 andesite inclusions are characterized by minor compositional zonation, which implies crystallization from a liquid reservoir that was very large compared to the degree of crystallization. The crystals have closely spaced, euhedral, fine-scale (+/–2 mol% An) oscillatory zones and minor to abundant dissolution surfaces in places associated with abrupt changes in composition of up to 10 mol% An. Compositional and textural features such as these are exceedingly common in volcanic plagioclase phenocrysts (e.g. Anderson 1984; Nixon and Pearce 1987; Pearce et al. 1987; Singer et al. 1993 1995; Pearce 1994). Euhedral, oscillatory zones are normally thought to reflect diffusion-controlled processes within the local environment of the growing crystal (e.g. Sibley et al. 1976; Haase et al. 1980, Allègre et al. 1981; Pearce and Kolisnik 1990) whereas repetitive dissolution surfaces are best explained by small scale fluctuations in temperature during crystal growth (e.g. Pearce 1994). These observations have most recently been attributed to crystallization within a dynamic environment where cyclical, small scale changes in temperature during convective crystal cycling lead to repetitive periods of crystal growth and dissolution (e.g. Singer et al. 1993 1995; Pearce 1994). Altogether, the textural and compositional features of the andesite inclusion and its constituent plagioclase phenocrysts indicate growth within a dynamic, largely crystal-free body of andesite magma. The presence of occasional dissolution surfaces, most of which are characterized by only small (<2 mol% An) discontinuous jumps in An content suggests that the andesite body may have been undergoing weak convection (e.g. Homma 1932; Singer et al. 1995)

In contrast to the andesite phenocrysts, plagioclase crystals in the gabbros have smooth, progressive rimward variations in both major and trace element abundances. The cumulate plagioclase phenocrysts display little to no oscillatory zonation. Most importantly, these crystals completely lack dissolution surfaces. As pointed out by Pearce and Kolisnik (1990), textures that lack dissolution surfaces are very rare among volcanic plagioclase phenocrysts, which suggests crystallization in a fundamentally different environment from that in which volcanic phenocrysts are grown. We interpret the smooth, featureless textures of the cumulate gabbro crystals as indicative of crystallization in a quiescent environment in which the small scale temperature fluctuations that are seemingly necessary for repetitive crystal dissolution (Pearce 1994) are absent. Altogether, the textural and compositional features of the hornblende gabbro inclusions and their constituent plagioclase crystals indicate a process of in situ fractional crystallization within a stagnant environment that underwent steady, progressive, internal differentiation. The most likely environment is that of a stagnant, thermally generated magmatic boundary layer somewhere along the margins of a body of parental andesite magma (e.g. McBirney et al. 1985; Marsh 1989; Langmuir 1989; Jaupart and Tait 1995). The textural and compositional characteristics of the plagioclase crystals require that little to no movement of the interstitial liquid occurred within the boundary layer prior to melt extraction and eruption.

Implications for the interpretation of trace element zonation profiles

A basic tenet in trace element partitioning theory is that the amount of a trace element that is incorporated into a growing crystal is controlled, in part, by the concentration of the element in the liquid at the crystal-liquid interface. Shimizu (1983) has shown that crystal growth generates a liquid compositional boundary layer around the crystal, and that the liquid concentration of a given trace element within the boundary layer, and especially at the crystal-liquid interfac, is significantly different from its concentration in the liquid beyond the outer edge of the compositional boundary layer. Thus, the core-to-rim variation in trace element abundance preserves a temporal record of what happened within the compositional boundary layer, not the large-scale liquid reservoir as a whole, and *cannot* be used to reconstruct large-scale liquid composition changes as a function of time.

This conclusion is at odds with our own study, which has shown that the core-to-rim variations in trace element abundance in plagioclase appear have indeed recorded the progressive, large-scale (i.e. on the scale of the entire magmatic boundary layer) fractionation of an interstitial boundary layer liquid. How, then, can the theory and our observations be reconciled? One option is that buoyancy-driven convection of the interstitial liquid was occurring through a permeable magmatic boundary layer and that it was sufficiently vigorous to continuously strip away the compositional boundary layers around each and every crystal. However, the compositional and textural features of the plagioclase crystals (Fig. 3 and 4) clearly argue against any environment in which significant movement of the interstitial liquid occurred prior to extraction and eruption. An alternative explanation, and one that we favor, is that following an initial period of crystal nucleation and rapid crystal growth at the leading edge of an inward solidifying magmatic boundary layer, the bulk of the plagioclase crystallization occurred within the partially to eventually largely solidified region of the magmatic boundary layer. During this time, the cool-

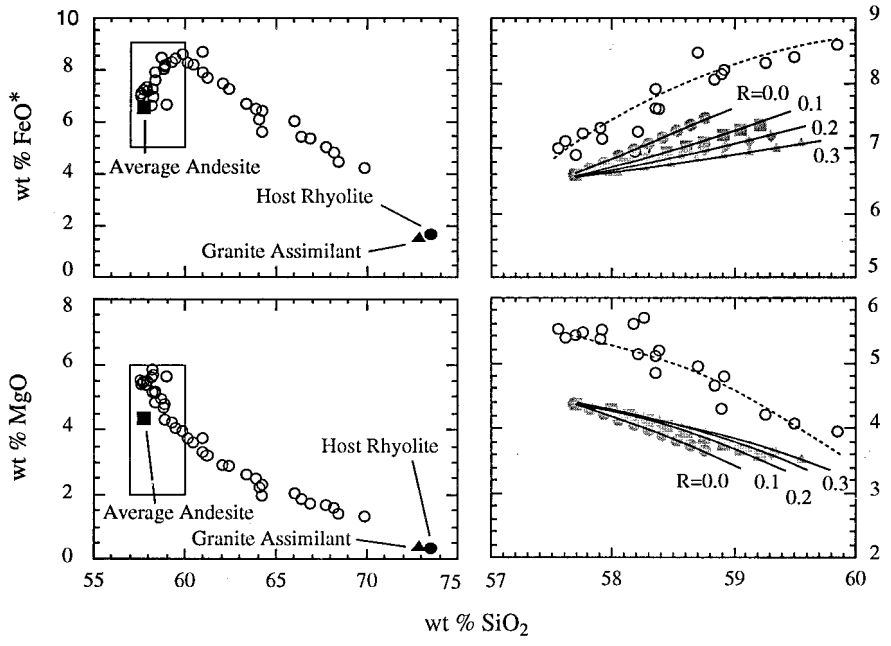

Fig. 7 Results of open-system AFC calculations assuming a bulk assimilant equivalent to the average of the granitic xenoliths reported in Table 1. The left hand side of the diagram displays the predicted co-variation in liquid FeO* and MgO with increasing SiO_2 for the mantle of 1555M-A. along with the observed compositions of the average andesite inclusion, host rhyolite and assumed granitic assimilant. The right-hand diagrams display, for both FeO* and MgO, the predicted liquid compositions for Stage I crystallization along with calculated AFC paths for increasing values of R (mass assimilated/mass crystallized). The *dashed lines* represent the approximated variation in predicted liquid abundances. The fractionation calculations are based on the method of Grove and Donnelly-Nolan (1986) and assume a parental magma equivalent to the average of the quenched andesite inclusions. Note that, in both cases, the slope of the calculated variation agrees best with the slope of the predicted variation for 0% crustal assimilation (i.e. R=0.0). These results suggest that fractional crystallization occurred under closed system conditions

ing rate was sufficiently slow that plagioclase growth rates were significantly less than chemical diffusion rates in the liquid. In this case, rapid diffusion of chemical species towards a slowly advancing crystal-liquid interface could forestall the development of a significant compositional boundary layer around individual crystals, and thus ensure that the liquid composition at the crystal-liquid interface was close to that of the liquid reservoir as a whole. Significantly, Cashman and Marsh (1988) have estimated plagioclase phenocryst growth rates at around 10^{-11} cm/s whereas chemical diffusion rates in silicate melts are typically on the order of 10^{-9} to 10^{-10} cm^2/s (e.g. Donaldson 1975; Baker 1992). These growth rates are indeed smaller (but only by a few orders of magnitude) than typical chemical diffusivities and would seem to support our suggestion. However, without detailed knowledge of the thermal history of the two gabbro inclusions, which is critical for estimating true plagioclase growth rates, it is impossible to draw any firm conclusions.

Closed- versus open-system crystallization

Grove and Donnelly-Nolan (1986) have demonstrated on trace element grounds that the andesite fractionation that generated the host rhyolite must have been accompanied by up to 30 wt% assimilation of granitic wall rock. If the fractional crystallization occurred within a quiescent magmatic boundary layer, obvious questions are how and when the required granitic component was incorporated. One possibility is that assimilation occurred during fractional crystallization (i.e. classical AFC, DePaolo 1981). An alternative possibility is that fractional crystallization and wallrock assimilation were separated in space and time and that the granitic component was added as a crustal melt after the fractionation had already taken place (e.g. Grove et al. 1988).

Based on textural observations, the crystallizing assemblages during the fractionation recorded by the gabbros were plagioclase+olivine+augite (Stage I) followed by plagioclase+hornblende+orthopyroxene+Fe-oxides+apatite and zircon (Stage II). If fractionation occurred under closed system conditions, these fractionation assemblages should lead to an initial period of FeO*-enrichment and MgO-depletion (Stage I) followed by subsequent FeO*- and continued MgO-depletion (Stage II). Both of these features are observed in the predicted liquid composition paths shown in Fig. 6. Simultaneous assimilation of large volumes of granitic wall-rock should diminish (or eliminate) the initial period of FeO*-enrichment and reduce the rate at which MgO decreases with increasing SiO_2. To test the possibility of closed- versus open-system fractionation during Stage I (and by inference Stage II) crystallization, a closed-system fractionation calculation was performed based on the procedure outlined in Grove and Donnelly-Nolan (1986). The initial parent magma and granitic as-

similant used in the calculation are based on the average of the low-SiO_2 andesite inclusions reported in Table 1 and Grove and Donnelly-Nolan (1986) and several analyses of granitic xenoliths from the rhyolite of Little Glass Mountain (Grove and Donnelly-Nolan 1986; Donnelly-Nolan, unpublished data).

The results of the calculation are shown in Fig. 7. The left side of Fig. 7 shows the variations in liquid FeO* and MgO from Fig. 6, as predicted from the mantle of crystal 1555M-A. The right side of Fig. 7 shows an enlarged view of the predicted Stage I liquid compositions along with the calculated liquid compositions for closed system (i.e. R=0, where R is mass assimilated/mass crystalized), and open system (R=0.1, 0.2 and 0.3) conditions. The calculated liquid compositions show that, as anticipated, the slope of both the FeO*-SiO_2 and MgO-SiO_2 variation decreases as progressively more granitic assimilant is added. A comparison of the predicted and calculated variations shows that the best agreement in the slope, if not the absolute abundances, is found for the case of closed-system crystallization (i.e. R=0.0). These results strongly imply that the magmatic boundary layer in which the hornblende gabbro cumulates were formed was chemically isolated from the surrounding wall-rock during crystallization. In this event, the necessary granitic component was added *following* extraction of the fractionation-generated liquid from the boundary layer environment. Thus, our results indicate that fractional crystallization and crustal assimilation did not occur simultaneously (i.e. the traditionally envisioned AFC process) but, rather, through a process in which the fractionation and assimilation were separated from one another in both space and time. Grove et al. (1988) have used different lines of evidence to advocate such a process beneath the Burnt Lava flow, located approximately 15 km to the southeast of Little Glass Mountain (Fig. 1). The similar results of these two studies in which the relative timing of fractionation and assimilation have been deduced indicates that the separation of fractionation and assimilation processes may be a common phenomenon where crustal assimilation is important.

A model of silicic magma generation at Little Glass Mountain

The most important conclusions of this study are: (1) the two hornblende gabbro inclusions record the progressive fractional crystallization of parental low-SiO_2 andesite magma through in situ processes in a quiescent magmatic environment (i.e. a crystallizing magmatic boundary layer); (2) fractional crystallization occurred under closed system conditions with little to no assimilation of crustal material during fractionation; and (3) a significant [more than 30% (Donnelly-Nolan, unpublished data)] crustal component was added to the final host rhyolite magma *after* extraction of the fractionation-generated silicic liquids. Based on these results, Fig. 8 summarizes a proposed model for the formation of the rhyolite of Little Glass Mountain. Intrusion of parental andesitic magma into granitic country rock led to cooling and crystallization through boundary layer solidification along the roof, walls, and floor. Closed-system boundary layer crystallization generated fractionated liquids that were trapped within the partially crystallized boundary layer. Heat from the crystallizing magma partially melted the granitic country rock in the vicinity of the intrusion. After some arbitrary period of time, the boundary layer sequence consisted of an inner rigid crust, defined by crystal contents of 50% or greater for low-SiO_2 andesite magma (Marsh 1981; Brophy 1991), and an outer mushy layer. Within this overall sequence, the interstitial liquids covered the entire liquid line of descent of the initial parental andesite and varied from around 56–57% SiO_2 at the inner margin of the boundary layer to around 74% SiO_2 at the original country rock contact. Fracturing of the rigid crust through local seismic activity, magmatic intrusion, or local foundering of the crust itself (e.g. Marsh 1995) led to extraction and accumulation of the silicic interstitial melt which then mixed with partially molten granitic country rock and erupted to form the rhyolite of Little Glass Mountain. The andesitic inclusions, gabbroic inclusions and granitic xenoliths are representative of the parental andesite magma, the depleted rigid crust, and partially molten country rock respectively. The specific gabbros studied must have come from somewhere in middle of the rigid crust (Fig. 8) as the observed and predicted interstitial liquids are around 70% SiO_2, which is 3 to 4 wt.% less than that of the final host rhyolite magma composition.

As drawn, Fig. 8 suggests that the host rhyolite lava, andesite inclusions, and cumulate gabbro inclusions necessarily were derived from the same body of magma. Though this is possible, trace element data from the andesite inclusions (Grove and Donnelly-Nolan 1986) seem to indicate the presence of at least two unrelated andesite magmas. This suggests a process in which a pre-existing body of rhyolite magma, generated through the process outlined in Fig. 8, is intruded by successive injections of different composition andesite magma. The rhyolite magma probably already contained genetically related hornblende gabbro entrained during extraction of the rhyolitic melt, plus xenoliths of partially molten granitic wall rock incorporated during assimilation and mixing of the rhyolite and melted granitic liquids. The intruded andesites could have commingled with the rhyolite to generate magmatic andesite inclusions, perhaps along the lines originally envisioned by Eichelberger (1981) for the nearby Glass Mountain rhyolite lava. Nevertheless, Fig. 8 summarizes what we believe to be the general magmatic relations between rhyolite, andesite, granitic country rock, and gabbro cumulates beneath Little Glass Mountain.

Though ultimately impossible to determine, it is tempting to speculate on the specific location of the boundary layer from which the silicic magma was extracted. The hornblende gabbro xenoliths record in situ crystallization in a static magmatic boundary layer. In

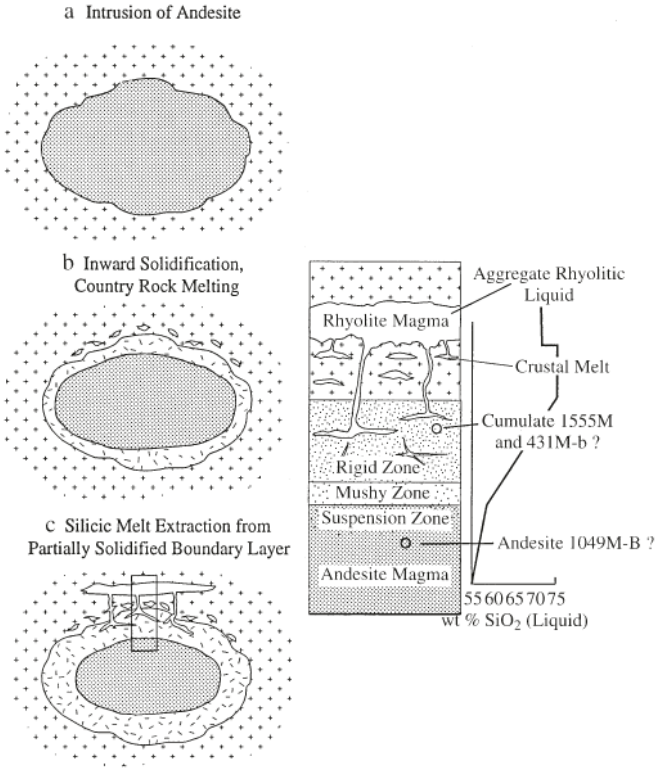

Fig. 8 Schematic diagram of the proposed model of silicic melt generation beneath Little Glass Mountain. See text for discussion

calc-alkaline systems, crystallization leads to a progressive decrease in liquid density. In a magmatic boundary layer located along the chamber floor, evolved low-density liquids may lie beneath less-evolved, higher density liquids. Along the wall, evolved low density liquids will lie adjacent to less evolved high density liquids. In both situations gravitational instability of the liquid should lead to compositional convection through permeable regions of the boundary layer (e.g. Jaupart and Tait 1995). Movement of the interstitial liquid would lead to dynamic rather than quiescent conditions during crystallization. As considered above, the textural and compositional features of the cumulate plagioclase crystals do not support such a conclusion. In contrast, a magmatic boundary layer beneath the roof should contain interstitial liquids that are gravitationally stable. Compositional convection should be absent and crystallization should proceed under quiescent conditions, which agrees with our own observations. Thus, we favor a process of melt extraction from the roof sequence of the crystallizing andesite magma body.

Implications for the formation of fractionation-generated composition gaps

Numerous models have been suggested for the origin of fractionation-generated composition gaps. These include:

(1) a liquid density or viscosity maximum that prohibits the eruption of a specific range of magma compositions (e.g. Baker et al. 1977; Jones 1979);

(2) sidewall crystallization, compositional convection, and collection of evolved liquid at the top of a magma body (i.e. liquid fractionation, McBirney et al. 1985);

(3) closed system fractional crystallization in a vigorously convecting magma body accompanied by crystal retention, crystal congestion, cessation of convection, and eventual melt extraction from a rigid crystal-liquid mush (Brophy 1991);

(4) closed system fractional crystallization of quiescent magma with eventual melt extraction after the entire body consists of a rigid crystal-liquid mush (Thompson 1972); and

(5) closed system boundary layer solidification beneath the roof of a magma body followed by melt extraction accompanying sagging or internal tearing of the rigid crust (i.e. solidification front instability, Marsh 1995).

Based on Fig. 8, we suggest that the fractionation-generated composition gap at Little Glass Mountain formed through a process similar to (4) or (5) above, wherein all fractionation takes place within magmatic boundary layers. The fractionating interstitial liquid is held within the boundary layer until the layer itself becomes rigid enough to permit fracturing and melt extraction. In this fashion, a significant portion of the parental magma liquid-line-of-descent is effectively prohibited from reaching the surface, thus forming a composition gap on the surface. If melt extraction is indeed from a boundary layer located beneath the roof of the magma body, as suggested above, then the general solidification front instability model of Marsh (1995) may be the most applicable here.

Phase equilibria controls on the composition gap formation

Several authors have proposed that fractionation-generated composition gaps are due to the appearance of a new liquidus mineral that causes a fractionating magma to pass rapidly through a certain composition interval (i.e. SiO_2), thus reducing the probability that magmas within that composition range are erupted onto the surface. Suggested minerals include an Fe-oxide phase (Mukherjee 1967; Weaver 1977; Clague 1978) and/or various mafic mineral/melt reaction products such as amphibole or orthopyroxene (Grove and Donnelly-Nolan 1986). Figure 9 shows plots of An content (mole%) and Fe abundance (ppm) in plagioclase versus the cube of the distance from the rim (m^3) of the mantle of 1555M-A. Also plotted is the predicted variation in liquid SiO_2 content from the same crystal. If the crystal grew at a constant rate, the volume of the crystal increases at a rate proportional to the cube of the crystal radius, r. Thus, any change in the slope of a given geochemical parameter when plotted against r^3 should indicate a change in the

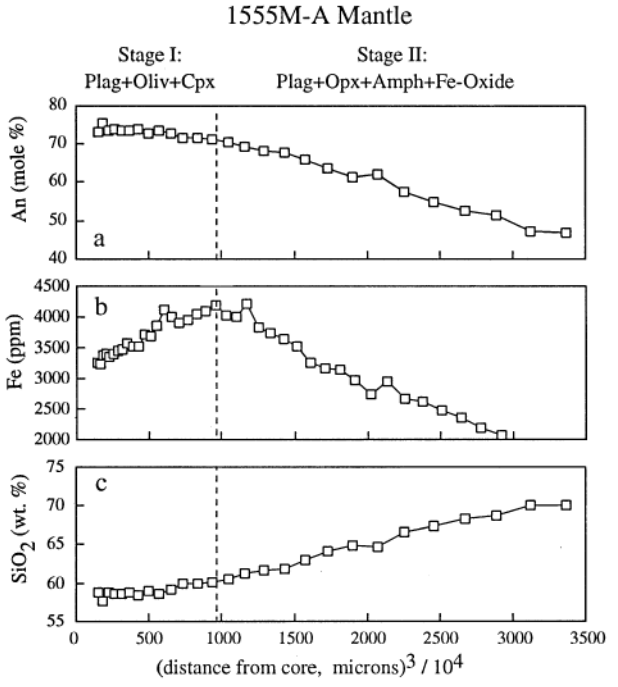

Fig. 9a–c An content (mol%) and Fe abundance (ppm) in plagioclase, and predicted liquid SiO_2 from the mantle of 1555M-A versus the cube of the distance from the core (mm). The boundary between Stage I and Stage II crystallization is marked by the inflection point in the Fe profile. Note the systematic increase in predicted liquid SiO_2 during crystal growth, which suggests a constant rate of increase in liquid SiO_2 during fractionational crystallization

rate at which that parameter is changing in the liquid (Pearce et al. 1987). The mantle of 1555M-A records the crystallization of plag+oliv+cpx (Stage I) followed by plag+opx+amph+Fe-oxide (Stage II). Significantly, the beginning of Stage II is marked by the appearance of all three minerals that have been invoked to explain a composition gap. Thus, if the phase equilibria model is correct, there should be a significant increase in the slope of the predicted liquid SiO2 variation at the onset of Stage II crystallization. The Fe profile shows where the transition from Stage I to Stage II crystallization occurs in 1555M-A. In the liquid SiO_2 profile the transition from Stage I to Stage II shows only a *very* slight increase in slope. This suggests that the appearance of these minerals did not dramatically increase the rate of change of SiO_2 in the liquid, a result that argues against the phase equilibria explanation for the formation of a composition gap. Thus, we conclude that the most reasonable explanation for the formation of a fractionation generated composition gap beneath Little Glass Mountain (and other volcanic systems?) is the physical model of boundary layer crytallization and eventual melt extraction proposed in Fig. 8.

Conclusions

The rhyolite of Little Glass Mountain and associated cumulate hornblende gabbro and quenched andesite liquid inclusions represents a situation where all three components of a fractional crystallization event that produced a composition gap have been preserved in a single volcanic eruption. This occurrence provides an opportunity to evaluate the potential processes that generate a composition gap and, in turn, the physical mechanisms of fractional crystallization in general. Through the combined analysis of textural (NDIC) and compositional (major and selected trace element) zonation styles in plagioclase phenocrysts from the parental andesite magma (quenched andesite inclusions) and fractionation-generated cumulate residue (hornblende gabbro inclusions), we conclude that the most likely mechanism of fractional crystallization that generated the host rhyolite lava is one of inward solidification of a crystallizing boundary layer along the margins of an andesitic body of magma followed by melt extraction, accumulation and eruption of the highly evolved interstitial liquid. The proposed mechanism of inward solidification and melt extraction fully explains the formation of the composition gap that is observed between the parental andesite and derivative rhyolite magma compositions. Finally, perhaps the most significant aspect of this work is the demonstration that the combined analysis of major and trace element zonation profiles coupled with detailed textural information of individual crystals provides a very powerful tool for deciphering igneous magmatic processes.

Appendix

Fractional crystallization leads to a correlation between liquid SiO_2 (in wt%), liquid Ca/Na (mol%) and plagioclase An content (mol%). Due to insufficient information on the differentiation pressure as well as the H_2O content of the parental andesite magma beneath Little Glass Mountain, it is impossible to determine rigorously the magmatic SiO_2-equilibrium plagioclase composition relationship. Thus, an alternative approach has been adopted for reconstructing liquid SiO_2 contents.Grove and Donnelly-Nolan (1986) and Donnelly-Nolan et al. (1990) have shown that the compositional variations among the late Holocene lavas of intermediate to silicic composition that were erupted during the same general time period as the Little Glass Mountain rhyolite are due largely to low-pressure fractional crystallization. If the compositional variation of the erupted lavas is assumed to represent the general fractionation-generated liquid-line-of-descent beneath Medicine Lake Volcano during the late Holocene, then the compositional variations recorded by the erupted lavas should be roughly equivalent to that followed by the liquid during the fractionation process recorded by the two gabbros. Figure A1a shows the variation in whole-rock SiO_2 versus Ca/Na ratio for late Holocene mafic to silicic lavas from Medicine Lake Volcano (Donnelly-Nolan et al. 1990), which, for the intermediate to silicic lavas at least, is taken as being representative of the likely variation in magmatic (i.e. liquid) SiO_2 and Ca/Na. Figure A1b shows the variation between magmatic SiO_2 content and predicted equilibrium plagioclase composition, where the magmatic Ca/Na ratios have been converted to equilibrium plagioclase composition using a plagioclase-liquid Ca/Na K_D value of 2.5 which has been shown to be appropriate for the Medicine Lake lavas (Grove and Donnelly-Nolan 1986). A third-order polynomial curve, that has been fit to the data in Fig. A1b is assumed to represent the general relationship between liquid SiO_2 abundance and plagioclase composition during the fractionation process recorded by the plagioclase crystals of the two gabbros.

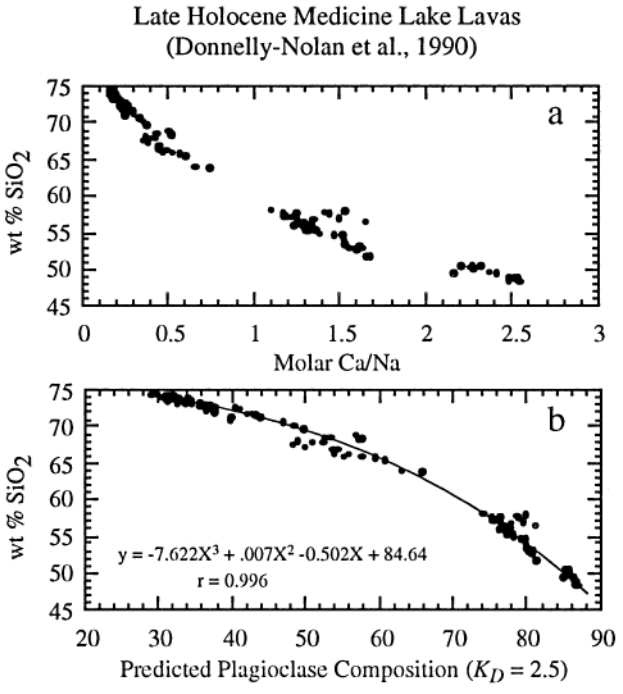

Fig. A1 **a** Plot of whole rock SiO_2 (wt%) versus Ca/Na (molar) for late-Holocene lavas from Medicine Lake plotted in Donnelly-Nolan et al. (1990) **b** Plot of whole rock SiO_2 (wt%) versus predicted equilibrium plagioclase composition where the latter has been calculated from the molar Ca/Na ratio assuming a plagioclase-liquid Ca/Na K_D of 2.5 as suggested by Grove and Donnelly-Nolan (1986) The solid line represents a third order polynomial best fit curve through the data ($y=-7.622\times10^{-5}(x^3)+7.613\times10^{-3}(x^2)-5.019\times10^{-1}(x)+84.64$ ($r=0.996$)). It is assumed that this curve represents the general relationship between fractionation-related liquid SiO_2 abundances and equilibrium plagioclase composition for all Medicine Lake magmas, including those present during the fractional crystallization recorded by the plagioclase crystals of the two hornblende gabbro cumulates

Acknowledgements This work was supported by NSF-9117246 (Brophy). The senior author wishes to thank Nobu Shimizu, Charles Bacon, Tom Sisson, and an unidentified reviewer for critical but thoughtful reviews that materially improved the presentation and discussion of our results. Thanks are also extended to the various analytical chemists in the U.S.G.S. for providing the geochemical data used in the study.

References

Allegre CJ, Provost A, Jaupart C (1981) Oscillatory zoning: a pathological case of crystal growth. Nature 294: 223–294

Anderson CA (1933) Volcanic history of Glass Mountain, northern California. Am Jour Sci, 26: 485–506

Anderson CA (1941) Volcanoes of the Medicine Lake Highland, California. Univ Calif Publ Geol Scil, 25: 347–422

Anderson AT Jr (1984) Probable relations between plagioclase zoning and magma dynamics, Fuego volcano, Guatemala. Am Mineral 69: 670–676

Bacon CR, Druitt TH (1983) Compositional evolution of the zoned calc-alkaline magma chamber of Mount Mazama, Crater Lake, Oregon. Contrib Mineral Petrol 98: 224–256

Baker DR (1992) Estimation of diffusion coefficients during interdiffusion of geologic melts: Application of transition state theory. Chem Geol 98: 11–21

Baker BH, Goles GG, Leeman WP, Linstrom MM (1977) Geochemistry and petrogenesis of a basalt-benmoreite-trachyte suite from the southern part of the Gregory Rift, Kenya. Contrib Mineral Petrol 64: 303–332

Brophy JG (1991) Composition gaps, critical crystallinity, and fractional crystallization in orogenic magmatic systems. Contrib Mineral Petrol 109: 173–182

Brophy JG, Allan JF (1993) Textural and mineralogic studies of plagioclase phenocrysts from ODP Leg 142, Site 864A: implications for magmatic processes beneath the East Pacific Rise (EPR), 9°30′N. EOS Trans Am Geophys Union 744: 644

Blundy JD, Wood BJ (1991) Crystal-chemical controls on the partitioning of Ba and Sr between plagioclase feldspar, silicate melts and hydrothermal solutions. Geochim Cosmochim Acta 55: 193–209

Cashman KV, Marsh BD (1988) Crystal size distribution (CSD) in rocks and the kinetics and dynamics of crystallization II: Makaopuhi Lava Lake. Contrib Mineral Petrol 99: 292–305

Ciancanelli EV (1983) Geology of Medicine Lake volcano. Trans Geotherm Res Counc 7: 135–140

Clague DA (1978) The oceanic basalt-trachyte association: an explanation of the Daly Gap. Jour Geol 86: 739–743

Condie KD, and Hayslip DL (1975) Young bi-modal volcanism at Medicine Lake volcanic center, northern California. Geochim Cosmochim Acta 39: 1165–1178

Crawford AJ, Green HG, and Exon NF (1987) Geology, petrology and geochemistry of submarine volcanoes around Epi island, New Hebrides island arc. In: Green HG, Wong FL (eds) Geology and offshore resources of Pacific island arcs - Vanuatu region. Earth Science Series 8. Circum-Pacific Council for Energy and Mineral Resources. Houston, TX, pp 301–327

Daly RA (1925) The geology of Ascension Island. Proc Am Acad Arts Sci 60: 1–80

DePaolo DJ (1981) Trace element and isotopic effects of combined wallrock assimilation and fractional crystallization. Earth Planet Sci Lett 53: 189–202

Donaldson CH (1975) Calculated diffusion coefficients and the growth rate of olivine in a basalt magma. Lithos 205: 163–174

Donnelly-Nolan JM (1988) A magmatic model of Medicine Lake volcano, California. Jour Geophys Res 93: 4412–4420

Donnelly-Nolan JM Champion DE, Miller CD, Grove TL, Trimble DA (1990) Post-11|000-year volcanism at Medicine Lake volcano, Cascade Range, northern California. Jour Geophys Res 85: 19693–19704

Donnelly-Nolan JM, Champion DE, Grove TL, Baker MB, Taggart JE. Jr, Bruggman PE (1991) The Giant Crater Lava Field: geology and geochemistry of a compositionally zoned, high alumina basalt to basaltic andesite eruption at Medicine Lake volcano, California. J Geophys Res 96: 21843–21863

Eichelberger JC (1975) Origin of andesite and dacite: evidence of mixing at Glass Mountain in California and at other circum-Pacific volcanoes. Geol Soc Am Bull 86: 1381–1391

Eichelberger JC (1981) Mechanism of magma mixing at Glass Mountain, Medicine Lake Highland volcano, California. US Geol Surv Circ 838: 183–198

Gerlach DC, Grove TL (1982) Petrology of Medicine Lake Highland volcanics: characterization of the end members of magma mixing. Contrib Mineral Petrol 80: 174–159

Grove TL, Gerlach DG, Sando TW (1982) Origin of calc-alkaline series lavas at Medicine Lake Volcano by fractionation, assimilation and mixing. Contrib Mineral Petrol 80: 160–182

Grove TL, Donnelly-Nolan JM (1986) The evolution of young silicic lavas at Medicine Lake Volcano by fractionation, assimilation and mixing. Contrib Mineral Petrol 92: 281–302

Grove TL, Kinzler RJ, Baker MB, Donnelly-Nolan JM, Lesher CE (1988) Assimilation of granite by basaltic magma at Burnt Lava flow, Medicine Lake volcano, northern California: decoupling of heat and mass transfer. Contrib Mineral Petrol 99: 320–343

Haase CS, Chadam J, Feinn D, Ortoleva P (1980) Oscillatory zoning in plagioclase feldspar. Science: 272–274

Heiken G (1978) Plinian-type eruptions in the Medicine Lake Highland, California and the nature of the underlying magma. J Volcanol Geotherm Res 2: 1–16

Hildreth W (1983) The compositionally zoned eruption of (1912) in the Valley of Ten Thousand Smokes, Katmai National Park, Alaska. J Volcanol Geotherm Res 18: 1–56

Homma BF (1932) Uber das Ergebnis von Messungen an zonaren Plagioklasen aus Andesiten mit Hilfe des Universaldrehtisches . Schweiz Mineral Petrogr. Mitt 12: 346–352

Jaupart C, Tait S (1995) Dynamics of differentiation in magma resevoirs. J Geophys Res 100: 17615–17636

Jones WB (1979) The mixed benmoreite/trachyte flows from Kenya and their bearing on the Daly Gap. Geol Mag 116: 487–489

Langmuir CH (1989) Geochemical consequences of in situ crystallization. Nature 340: 199–205

Longhi J, Walker D, and Hays JF (1976) Fe and Mg in plagioclase. Proc Lun Sci Conf 7: 1281–1300

MacDonald R (1987) Quaternary peralkaline silicic rocks and caldera volcanoes of Kenya. In: Fitton JG, Upton BGJ (eds) Alkaline Igneous Rocks. Geol Soc London Spec Pub 30: 313–333

Marsh BD (1981) On the crystallinity, probability of occurrence, and rheology of lava and magma. Contrib Mineral Petrol 78: 85–98

Marsh BD (1989) Magma chambers. Ann Rev Earth Planet Sci 17: 439–474

Marsh BD (1995) Solidification fronts and magmatic evolution. Mineral Mag 60: 5–40

McBirney AR, Baker BH, Nilson RH (1985) Liquid Fractionation. Part I. Basic principles and experimental simulations. J Volcanol Geotherm Res 24: 1–24

Mertzmann SA (1977a) Recent volcanism at Schonchin and Cinder Buttes, northern California. Contrib Mineral Petrol 61: 231–243

Mertzmann SA (1977b) The petrology and geochemistry of Medicine Lake volcano. Contrib Mineral Petrol 62: 221–247

Mertzmann SA, Williams RJ (1981) Genesis of recent silicic magmatism in the Medicine Lake Highland, California: Evidence from cognate inclusions found at Little Glass Mountain. Geochim Cosmochim Acta 45: 1463–1478

Meyer PS, Shibata T (1990) Complex zoning in plagioclase feldspars from ODP Site 648. Proc Ocean Drill Prog Sci Res 106/109: 123–142

Mukherjee A (1967) Role of fractional crystallization in the descent: basalt - trachyte. Contrib Mineral Petrol 16: 139–148

Nixon GT, Pearce TH (1987) Laser interferometry study of oscillatory zoning in plagioclase: the record of magma mixing and phenocryst recycling in calc-alkaline magma chambers, Ixtaccihuatl volcano, Mexico. Am Mineral 72: 1144–1162

Pearce TH (1994) Recent work on oscillatory zoning in plagioclase. In Parsons I (ed) Feldspars and their reactions. Kluwer Academic Publishers, pp 313–349

Pearce TH, Kolisnik AM (1990) Observations of plagioclase zoning using interference imaging. Earth Sci Rev 19: 9–26

Pearce TH, Griffin MP, Kolisnik AM (1987) Magmatic crystal stratigraphy and constraints on magma chamber dynamics: laser interference results on individual phenocrysts. J Geophys Res 92: 13745–13752

Phinney WC (1991) Partition coefficients for Fe, Mg, Ti, and K between plagioclase and basalt: Implications for anorthosites: Lunar Plan. Sci Conf Ext Abstr 22: 18–22

Phinney WC, Morrison DA (1990) Partition coefficients for calcic plagioclase: Implications for Archean anorthosites. Geochim Cosmochim Acta 54: 1639–1654

Pouchou JL, and Pichoir F (1985) PAP (phi-rho-z) procedure for improved quantitative microanalysis. In: Armstrong JT (ed) Microbeam analysis. San Francisco Press, San Francisco, pp 104–106

Powers HA (1932) The lavas of the Modoc Lava-Bed quadrangle, California. Am Mineral 17: 253–294

Sato H (1989) Mg-Fe partitioning between plagioclase and liquid in basalts of hole 504B, ODP Leg 111: a study of melting at 1 atm. Proc Ocean Drill Prog Sci Results 111: 17–26

Shimizu N (1983) Interface kinetics and trace element distribution between phenocrysts and magma. In: Augustithus S (ed) The significance of trace elements in solving petrogenetic problems and controversies. Theophrastus, Athens, pp 175–(195

Shimizu N, Hart SR (1982) Application of the ion micro-probe to geochemistry and cosmochemistry. Ann Rev Earth Plan Sci 10: 483–526

Sibley DF, Vogel TA, Walker BM, Byerly G (1976) The origin of oscillatory zoning in plagioclase: a diffusion and growth model. Am Jour Sci 276: 275–284

Singer BS, Pearce TH, Kolisnik AM, Myers JD (1993) Plagioclase zoning in mid-Pleistocene lavas from the Seguam volcanic center, central Aleutian arc, Alaska. Am Mineral 87: 143–157

Singer BS, Dungan MA, and Layne GD (1995) Textures and Sr, Ba, Mg, Fe, K and Ti compositional profiles in volcanic plagioclase: clues to the dynamics of calc-alkaline magma chambers. Am. Mineral, 80, 776–798

Smith AL, Carmichael ISE (1968) Quaternary lavas from the sourthern Cascades, western USA. Contrib Mineral Petrol 19: 212–238

Thompson RN (1972) Evidence for a chemical discontinuity near the basalt-andesite transition in many anorogenic volcanic suites. Nature 236: 106–110

Wagner TP, Donnelly-Nolan JM, Grove TL (1995) Evidence of hydrous differentiation and crystal accumulation in the low-MgO, high-Al_2O_3 Lake Basalt from Medicine Lake volcano, California. Contrib Mineral Petrol 121: 201–216

Weaver SD (1977) The quaternary caldera volcano Emuruangogalak, Kenya Rift, and the petrology of a bimodal ferrobasalt-pantelleritic trachyte association. Bull Volcanol 40: 209–227

Weaver SD, Saunders AD, Pankhurst RJ, Tarney J (1979) A geochemical study of magamtism associated with the initial stages of back-arc spreading: the Quaternary volcanics of Bransfield Strait, from South Shetland Islands. Contrib Mineral Petrol 68: 151–169